

Article

Development and Research of New Hybrid Composites in Order to Increase Reliability and Durability of Structural Elements

Peter Rusinov ^{*}, Zhesfina Blednova, Anastasia Rusinova, George Kurapov  and Maxim Semadeni

Department of Engineering of Control Systems, Materials and Technologies in Mechanical Engineering, Kuban State Technological University, Krasnodar 350072, Russia; blednova@mail.ru (Z.B.)

* Correspondence: ruspiter5@mail.ru

Abstract: Hybrid composite materials can successfully solve the problems of reliability, durability, and extended functionality of products, components, and details, which operate under conditions of multifactorial influences (temperature, force, and deformation). The authors have developed a hybrid composite high-entropy AlCoCrCuFeNi material and ceramic cBNCoMo(B₄CCoMo) layer. The formation of hybrid composites was carried out using new technology. This technology includes high-energy machining, high-velocity oxygen-fuel spraying in a protective environment, high-temperature thermomechanical treatment, and heat treatment. The use of the developed technology made it possible to increase the adhesive strength of the composite layers from 68 to 192 MPa. The authors performed an assessment of the structural parameters of the composite layers. The assessment showed that the composite layers had a nanocrystalline structure. The research included mechanical tests of the hybrid composites Hastelloy X (NiCrFeMo)—AlCoCrCuFeNi—cBNCoMo and Hastelloy X (NiCrFeMo)—AlCoCrCuFeNi—B₄CCoMo for cyclic durability (fatigue mechanical tests) and friction wear. The use of surface-layered materials AlCoCrCuFeNi—cBNCoMo and AlCoCrCuFeNi—B₄CCoMo in the composition of hybrid composites significantly increased cyclic durability. The use of surface-layered materials in the composition of hybrid composites made it possible to reduce wear intensity. The test results show that the developed composites are promising for use in various industries (including oil and gas), where high strength and wear resistance of materials are required.

Keywords: composite materials; ceramics; cyclic loading; high-cycle structural engineering; X-ray; fatigue; wear



Citation: Rusinov, P.; Blednova, Z.; Rusinova, A.; Kurapov, G.; Semadeni, M. Development and Research of New Hybrid Composites in Order to Increase Reliability and Durability of Structural Elements. *Metals* **2023**, *13*, 1177. <https://doi.org/10.3390/met13071177>

Academic Editor: Manoj Gupta

Received: 17 May 2023

Revised: 19 June 2023

Accepted: 22 June 2023

Published: 24 June 2023



Copyright: © 2023 by the authors. Licensee MDPI, Basel, Switzerland. This article is an open access article distributed under the terms and conditions of the Creative Commons Attribution (CC BY) license (<https://creativecommons.org/licenses/by/4.0/>).

1. Introduction

Correspondence between the properties of innovative materials and the increasingly stringent conditions for their operation is one of the most significant problems in modern industry. Most often, the weakest link in the “material—working environment” system, which determines the operating conditions and the resource of the entire system, is the surface. This is why it is important to develop methods and technologies for surface modification [1]. The composite design of surface layers is the most promising method for improving products operating under friction, cyclic loading, and exposure to active media. Materials with different functional and mechanical properties in the surface layer make the surface multifunctional, strong, heat-resistant, wear-resistant, erosion-resistant, corrosion-resistant, reliable, and durable [2].

High-entropy materials and ceramic wear-resistant materials as surface layers [3–13] or as part of surface composites [14–20] ensure an effective response to external factors and adaptation to external influences. High-energy technologies provide nanostructuring. At present, technologies for composite layered materials have already been developed. They include high-entropy layers and ceramic wear-resistant layers [2], which are formed using a multifunctional technological complex. The technologies for surface-layered composites

are mainly used to improve the properties of products [14–21]. Layered surface composites that have a range of properties are relevant for various industries (oil and gas, aerospace, mechanical engineering, etc.). Taking into account that materials of high hardness have low viscosity, it is necessary to create layered structures that provide damping and stress relaxation. Layers of high-entropy materials perform the functions of stress relaxation on the surface. In addition, stress relaxation in composite materials is achieved due to the correctly chosen “architecture” of the layered composite. Therefore, for example, the lower functional layer of the composite in contact with the base (Hastelloy X) should have greater plasticity and elasticity than the overlying layer. Moreover, the overlying layer in contact with the aggressive environment must have increased strength and hardness. Consequently, the chosen “architecture” provides high mechanical and functional properties to the composite material [15,21–24]. As a functional layer in a composite material, we chose a high-entropy material. As an overlying layer bordering the functional layer, we chose a combined ceramic material. This material is most suitable for contact media in the oil and gas industry. The functions of stress relaxation in a layered composite can also be performed by layers of high-entropy materials [25–31].

Hastelloy X (nickel–chromium–iron–molybdenum), which has proven itself in the oil and gas and petrochemical industries, has been chosen as the basis for improving the performance properties and wear resistance of surface-layered composites [32–35].

The aim of this work was to create surface-layered composites of AlCoCrCuFeNi—cBNCoMo and AlCoCrCuFeNi—B₄CCoMo with a range of properties. The composites will include a high-entropy material and a wear-resistant ceramic material that provide the desired functional and mechanical properties.

Research Objectives

- Substantiation of the choice of materials for hybrid composites (Section 2);
- Substantiation of the choice of equipment and technologies for the formation of hybrid composite materials (Section 2);
- Assessment of the influence of high-energy mechanical processing of powder materials AlCoCrCuFeNi, cBNCoMo, and B₄CCoMo on the quality and mechanical properties of composites (Section 2);
- Development of statistical models for optimizing the technological parameters of the formation of composite materials (Section 3.1);
- Study of the structure and structural parameters of composite materials after complex processing (Section 3.2);
- Study of the mechanical properties and fatigue testing of the obtained composites (Section 3.3);
- Testing of the developed composites for friction wear (Section 3.3);
- Substantiation of the choice of high-temperature thermomechanical treatment in order to improve the mechanical properties of composites (Section 4.1);
- Substantiation of the choice of the “architecture” of composite materials (Section 4.2).

2. Materials and Research Methods

2.1. Materials

The alloy Hastelloy X (NiCrFeMo) is widely used in the petrochemical industry. It was chosen as the basis [32–35]. The high-entropy AlCoCrCuFeNi alloy was chosen as the functional layer adjacent to the base (Hastelloy X (NiCrFeMo) alloy). The high-entropy AlCoCrCuFeNi alloy has high functional (superplasticity, etc.) and mechanical properties [36–40]. The combined ceramics cBNCoMo and B₄CCoMo, which have increased wear resistance and strength, were chosen as surface strengthening layers [41–43]. We chose high-velocity oxygen-fuel spraying (HVOF) as a source of thermal energy because it can form a fine-grained (nano) structure due to the extremely short time of interaction with the treated surface, i.e., due to high heating and cooling rates of the deposited material.

The chemical analysis of the studied powder compositions is presented in Table 1.

Table 1. Chemical analysis of materials, wt.%.

Material	Ni	Mo	Cr	Fe	W	Co	Mn	C	P	S	Si	Al	Ti	B	Cu	cBN	B4C
Hastelloy X	43.34	9.5	21.8	20.1	0.7	1.9	0.8	0.1	0.03	0.02	0.9	0.3	0.1	0.01	0.4	-	-
AlCoCrCuFeNi	16.7	-	16.7	16.7	-	16.7	-	-	-	-	-	16.6	-	-	16.6	-	-
cBNCoMo	-	5	-	-	-	10	-	-	-	-	-	-	-	-	-	85	-
B4CCoMo	-	5	-	-	-	10	-	-	-	-	-	-	-	-	-	-	85

2.2. High-Energy Machining

First, we implemented high-energy machining of the powder compositions. Then, we carried out high-velocity oxygen-fuel spraying in a protective environment. In order to improve the functional and mechanical properties of the composites AlCoCrCuFeNi—cBNCoMo and AlCoCrCuFeNi—B4CCoMo, we implemented high-energy machining of powder mixtures in a water-cooled centrifugal ball mill GEFEST-2 (AGO-2U). The ball mill has the following parameters: drum volume—150 cm³; ball acceleration—40 g ball ratio for loading (10–15):1; ball diameter—6 mm; ball material—WC; carrier speed—890 rpm; and drum speed—1000 rpm. We carried out high-energy machining in an inert environment (argon). We ran grinding and activation of powder compositions in the AGO-2 U ball mill in the field of three inertial forces: the Coriolis force and two centrifugal forces. The centrifugal forces acting on the balls and powder were many times higher than the force of gravity. This is why the powder was rapidly activated. We produced HVOF in a protective environment of wear-resistant layers cBNCoMo and B4CCoMo hybrid composites Hastelloy X (NiCrFeMo)—AlCoCrCuFeNi—cBNCoMo and Hastelloy X (NiCrFeMo)—AlCoCrCuFeNi—B4CCoMo after high-energy machining. The times for the high-energy mechanical processing of the powder materials were as follows: AlCoCrCuFeNi—20 min; B4CCoMo—30 min; and cBNCoMo—40 min. In the process of high-energy mechanical treatment, cBN and B4C particles are destructed by micro chipping. The powder particles acquire a rounded volumetric shape with a pronounced effect of mechanosynthesis. During high-energy mechanical processing, powder particles are stored in the energy released during the HVOF process. This increases the adhesion of the composite layers and the total quality of the layers (reduction of porosity).

2.3. Formation of Layered Composites

Before HVOF, AlCoCrCuFeNi, cBNCoMo, and B4CCoMo powders were dried in a vacuum oven for 3–6 h at a temperature of 120–180 °C. In order to increase the adhesion strength of the composite layers with the base (Hastelloy X alloy), we preliminarily sandblasted the surface of the Hastelloy X alloy.

We studied the microstructure with a JSM-7500 F super-resolution scanning electron microscope and a JEM-2100 transmission electron microscope. We studied the chemical formula of the materials with an Arcmet 8000 optical emission analyzer for metals and alloys and with an INCA X-sight energy-dispersive JSM-7500 F electron microscope. We measured the thicknesses of the layers with a DMS 2E thickness gauge. X-ray phase analysis was carried out using a Dron-7M device in Cu-K α radiation.

The high-temperature thermomechanical treatment of the AlCoCrCuFeNi, cBNCoMo, and B4CCoMo layers of Hastelloy X (NiCrFeMo)—AlCoCrCuFeNi—cBNCoMo and Hastelloy X (NiCrFeMo)—AlCoCrCuFeNi—B4CCoMo included plastic deformation at high temperatures and heat treatment (annealing). We carried out gradual plastic deformation of the AlCoCrCuFeNi, cBNCoMo, and B4CCoMo layers of Hastelloy X (NiCrFeMo)—AlCoCrCuFeNi—cBNCoMo and Hastelloy X (NiCrFeMo)—AlCoCrCuFeNi—B4CCoMo with a three-roller device (Figure 1b) in a protective environment (argon) at a temperature of 1173 K. This environment reduces the content of oxides in the layers. Oxides have a negative effect on the functional and mechanical properties of hybrid composite materials. The abovementioned device (Figure 1a) allowed ion cleaning of the product before the

layers' formation. This increases the adhesion strength of the layers to the base. After high-energy mechanical treatment of the AlCoCrCuFeNi, cBNCoMo, and B4CCoMo powders, which was followed by high-temperature thermomechanical treatment, the porosity of the layers decreased to 1%, and the adhesive strength increased up to 162–183 MPa. This increase can be explained by the combined effect on the sprayed material. This effect lies in HVOF in an argon environment and plastic deformation of the sprayed particles, accompanied by high particle velocity of the sprayed mechanically activated powder material and, consequently, by dynamic impact. The adhesive strength of the AlCoCrCuFeNi—cBNCoMo and AlCoCrCuFeNi—B4CCoMo composite materials deposited on the surface of the Hastelloy X (NiCrFeMo) superalloy without preliminary high-energy machining and high-temperature thermomechanical treatment was 65–68 MPa.

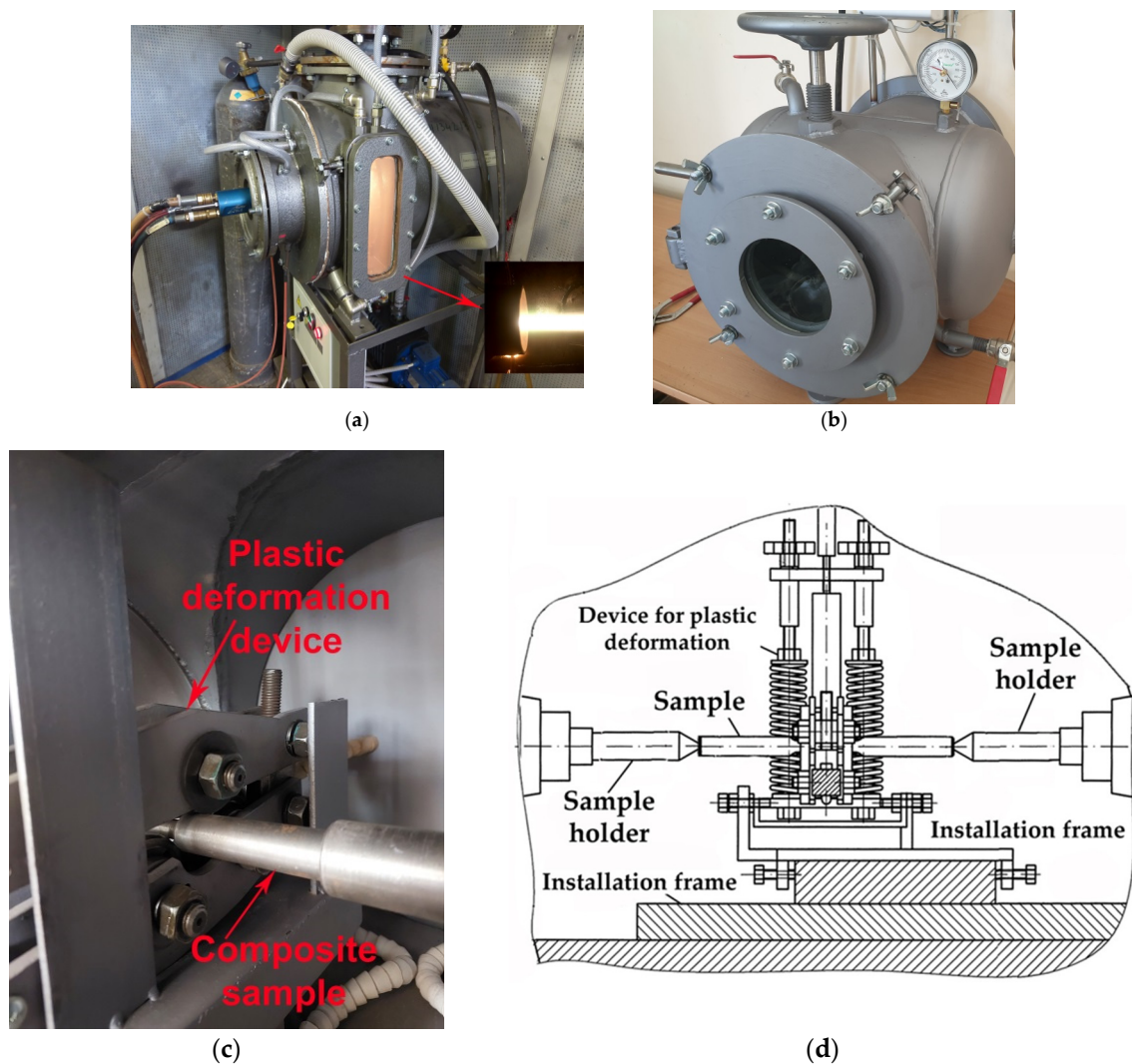


Figure 1. Multifunctional technological complex for the formation of hybrid composites in a protective environment—(a); machine for high-temperature thermomechanical treatment in a protective environment—(b); photograph of a device for high-temperature plastic deformation of materials—(c); scheme of a device for plastic deformation of materials—(d).

Plastic deformation of the materials was carried out by rolling on the laboratory device shown in Figure 1b–d. For plastic deformation of cylindrical samples, we used a special 3-roller device (rollers 50 mm in diameter, 8 mm wide) fixed in an installation case. The device allows for the processing of materials with a diameter of 8–20 mm with a contact load of up to 50 kN per roller. The device was calibrated using a DOS-0.1 dynamometer.

2.4. Mechanical Test

The microhardness of the layers was measured on a Falcon 503 device with a diamond pyramid with a 136° tip angle and an indenter load of 200 g. We examined porosity by hydrostatic weighing. We studied the properties of high-entropy coatings with experimental methods on special and standard equipment: on a fatigue test machine MUI-6000 and on a wear test machine 2070 SMT-1.

3. Results

When we form Hastelloy X—AlCoCrCuFeNi—cBNCoMo and Hastelloy X—AlCoCrCuFeNi—B4CCoMo using a multifunctional technological complex (Figure 1) and mechanically activated powders AlCoCrCuFeNi, cBNCoMo, and B4CCoMo, porosity decreases (pores are less than 0.8%), and adhesive and cohesive strength increases (162–183 MPa). An increase in the adhesive and cohesive strength of Hastelloy X—AlCoCrCuFeNi—cBNCoMo and Hastelloy X—AlCoCrCuFeNi—B4CCoMo can be explained by thermomechanical treatment (plastic deformation at a temperature of 1223–1323 K and subsequent annealing). This is also due to the formation of AlCoCrCuFeNi—cBNCoMo and AlCoCrCuFeNi—B4CCoMo by HVOF spraying. The increase can also be explained by the high-energy machining of applied materials.

We carried out annealing after we formed Hastelloy X—AlCoCrCuFeNi—cBNCoMo and Hastelloy X—AlCoCrCuFeNi—B4CCoMo in an inert medium at temperatures of 1073–1173 K. The annealing was carried out to eliminate excess intermetallic phases and reduce residual stresses after the layers' formation. After HVOF and annealing, we performed thermomechanical processing. This included plastic deformation at temperatures of 1223–1323 K, followed by annealing at temperatures of 973–1073 K for 1 h. Thermomechanical processing included plastic deformation of materials at high temperatures and subsequent annealing. Annealing of materials was carried out in order to relax stresses arising after plastic deformation. Plastic deformation of the materials was carried out under the pressure of the rollers on the surface of the material at a high temperature. Plastic deformation of the materials was carried out on the device shown in Figure 1b,c. Annealing of the hybrid layered composites was carried out at temperatures of 973–1073 K, depending on the composition of the alloy.

3.1. Design of Statistical Models for Hybrid Composites Using a Multifunctional Technological Complex

We used algorithmic planning and statistical processing of experimental data at all stages of the technological process: HVOF, annealing, and plastic deformation of the layers. In the search for the optimal technological regimens for hybrid composites using the experimental planning method, we adopted such a sequence of experiments that allows applying gradient search methods for an unknown function. This means that we approximately restored the law of object functioning according to the experimental data. When developing statistical models of the technological process, we used a uniform-rotatable plan. The following technological parameters were taken as the main ones: oxygen consumption, propane consumption, burner movement speed, spraying distance D , powder utilization factor E , spraying angle θ , residual argon pressure in the chamber P , etc. We considered the following output parameters: adhesive strength S (Equation (1)) and porosity P (Equation (2)). With these seven basic technological parameters, 92 experiments must be carried out to conduct a full-factorial experiment. Therefore, we accepted the values of the four main optimal parameters, based on the analysis of sources and the experience of previous studies: the flow rate of the carrier gas (argon)—45 L/min; spraying distance— D 220 mm; spraying angle— 80° ; rotation frequency of the coated part— 800 min^{-1} ; and residual pressure of argon in the chamber—0.7–0.8 Pa. An optimized assessment of the layers' characteristics (adhesion strength and porosity) allowed us to determine the optimal values: propane flow—80 L/min; oxygen—145 L/min; and burner speed—1.5 m/min. Based on the experience of previous studies, we selected the variation intervals of the studied fac-

tors: propane consumption—60–85 L/min; oxygen consumption—120–160 L/min; carrier gas consumption (argon)—40–50 L/min; distance between the torch and the processed material—D: 100–250 mm; spraying angle—70–90°; burner travel speed—1–1.5 m/min; rotation speed of the coated detail—800–1000 min⁻¹; residual pressure of argon in the chamber—0.7–0.8 Pa; and powder utilization ratio—E: 30–70%. Based on the results of statistical modeling of the technological process HVOF in the argon environment, we obtained regression equations (the variation interval of the factors $T_p = 209\text{--}2132\text{ }^\circ\text{C}$ and $V_p = 315\text{--}1156\text{ m/s}$). These equations express the dependence of coating quality characteristics and technological parameters of the process in the following Formulas (1) and (2):

$$S = 19.92 + 0.09 \times T_p - 0.09 \times V_p + 1.77 \times 10^{-6} \times T_p^2 - 9.28 \times 10^{-5} \times T_p \times V_p + 0.0002 \times V_p^2, \quad (1)$$

$$P = 29.22 - 0.007 \times T_p - 0.06 \times V_p + 1.45 \times 10^{-5} \times T_p^2 - 4.75 \times 10^{-5} \times T_p \times V_p + 8.05 \times 10^{-5} \times V_p^2, \quad (2)$$

where T_p is the temperature of the powder particles in $^\circ\text{C}$ and V_p is the speed of the powder particles in m/s.

A graphical interpretation of the response functions of adhesion strength and porosity is shown in Figure 2a,b. These parameters determine the main characteristics of the layers: adhesive and cohesive strength, level of residual stress, porosity, and structure.

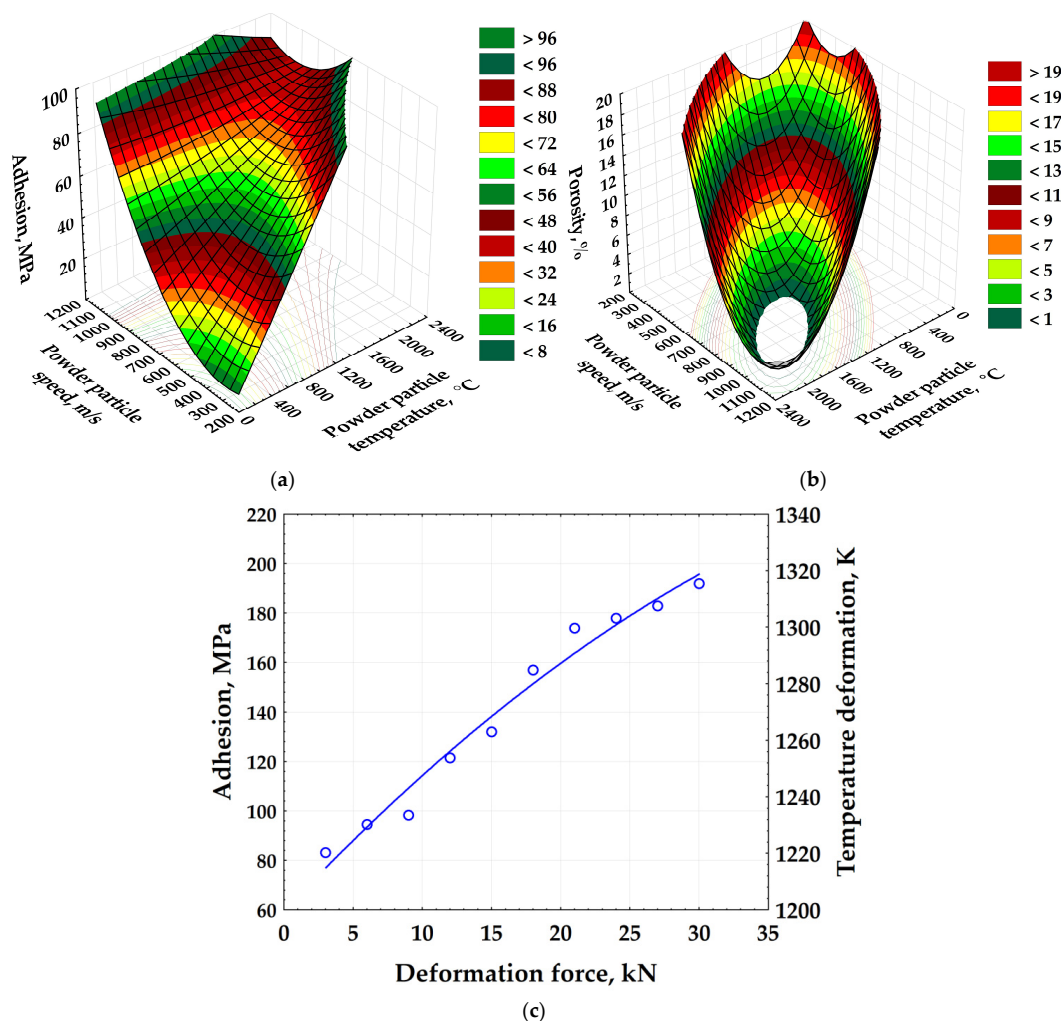


Figure 2. Dependence of adhesive strength (a) and porosity (b) on temperature and particle velocity of mechanically activated powder; material adhesion after high-temperature thermomechanical treatment—(c).

As a result of the analysis and mathematical processing of the experimental data, we obtained a polynomial curve of force dependence during deformation: temperature during deformation and adhesion of materials (Figure 2c). The highest adhesion of the surface composites AlCoCrCuFeNi—cBNCoMo(B4CCoMo) was achieved at a load of approximately 30 kN and a deformation temperature of 1316 K. When the load exceeded 30 kN, the base, which was Hastelloy X (NiCrFeMo) alloy, began to be pressed (deformed).

Experience shows that for high-velocity oxygen-fuel spraying in a protective environment, small powders (powder size less than 0.8 μm) cause technological difficulties. These difficulties lie in the burnout of individual components of the sprayed material in the gas flow. Therefore, the optimization of particle size distribution is one of the stages in the formation of “Hastelloy X—AlCoCrCuFeNi—ceramic material”. Statistical studies have shown that in order to obtain high-quality HVOF compositions in a protective environment, the optimal particle size distribution of the powder after high-energy mechanical processing is 0.9–15 microns. Powder particles with a finer fraction (less than 0.8 μm) stick together and violate the technological process (sticking of the powder dispenser channel).

3.2. Structure and Structural Parameters of Composite Materials

Macro- and microanalysis of Hastelloy X (NiCrFeMo)—AlCoCrCuFeNi—cBNCoMo and Hastelloy X (NiCrFeMo)—AlCoCrCuFeNi—B4CCoMo, obtained by the proven technology, showed that the structure of the layers was quite dense. The interface between the layers had no visible defects (Figure 3a–c). When powder particles pass through the gas-flame jet, they heat up and, upon impact with the substrate, harden in the form of deformed disks with a diameter of 1–12 μm and a thickness of 1–3 μm . The grain size in Hastelloy X—AlCoCrCuFeNi—cBNCoMo and Hastelloy X—AlCoCrCuFeNi—B4CCoMo obtained by HVOF is as follows: AlCoCrCuFeNi—75–123 nm (Figure 3d,e); cBNCoMo—92–136 nm (Figure 3f); and B4CCoMo—86–163 nm (Figure 3g). The thicknesses of Hastelloy X—AlCoCrCuFeNi—cBNCoMo and Hastelloy X—AlCoCrCuFeNi—B4CCoMo are AlCoCrCuFeNi—1–1.3 mm; cBNCoMo—0.5–0.7 mm; and B4CCoMo—0.5–0.7 mm. These thicknesses of the composite layers are optimal for the mechanical properties of hybrid composites.

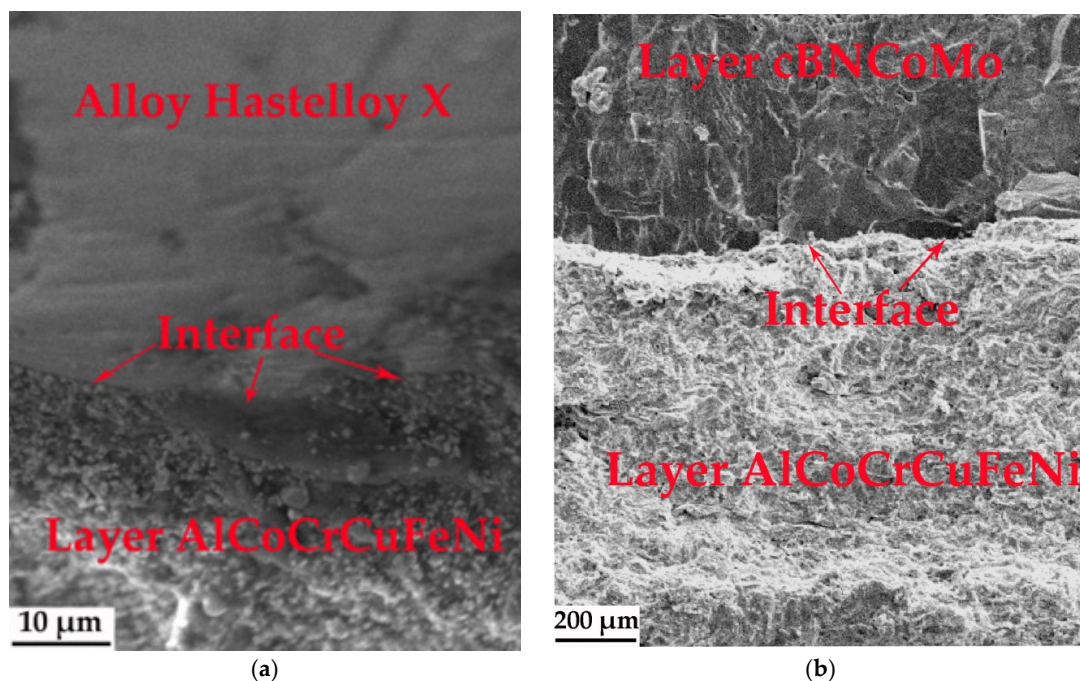


Figure 3. Cont.

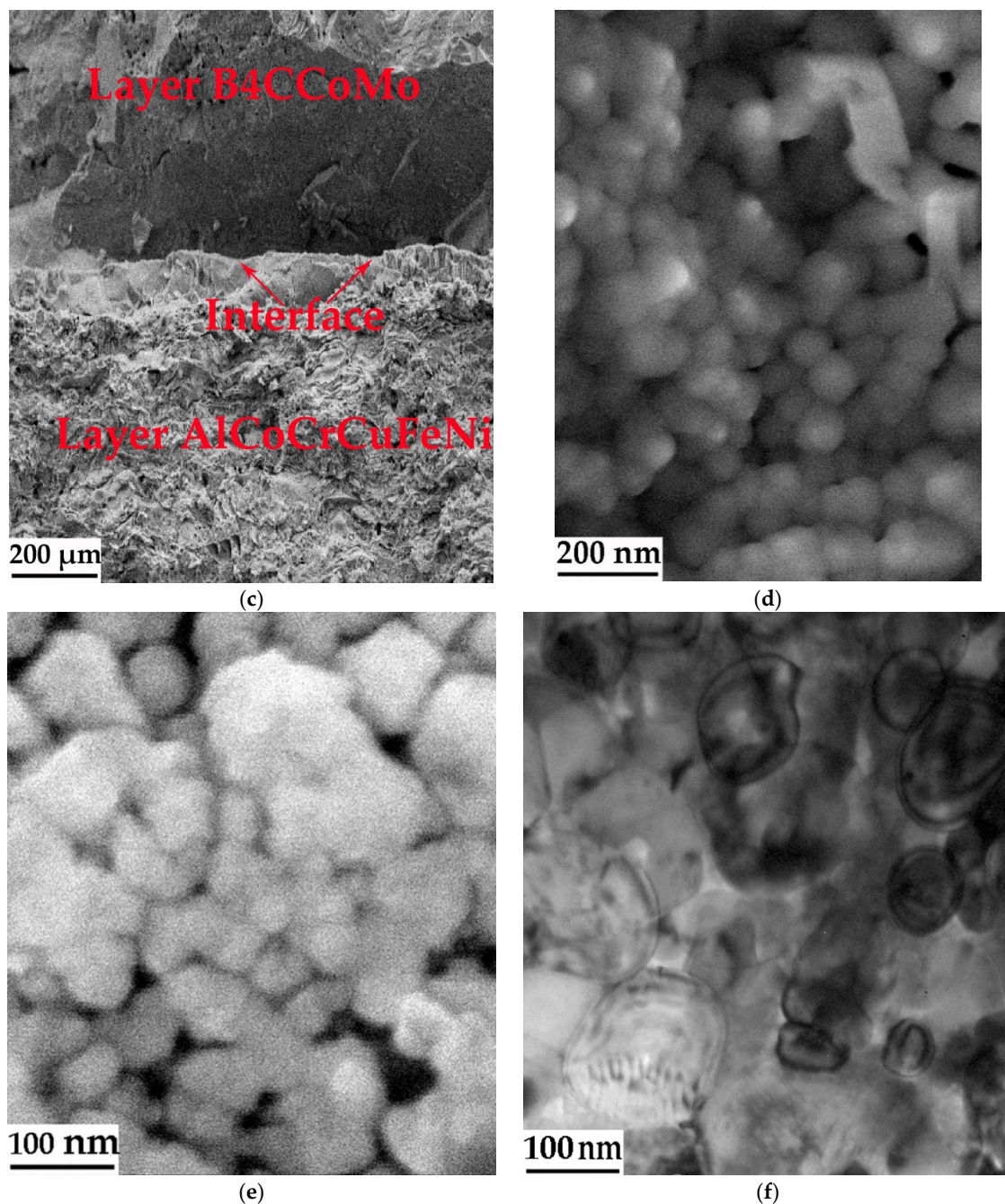


Figure 3. Structure and phase composition of Hastelloy X (NiCrFeMo)—AlCoCrCuFeNi—cBNCoMo and Hastelloy X (NiCrFeMo)—AlCoCrCuFeNi—B4CCoMo composites: (a) Hastelloy X—AlCoCrCuFeNi alloy structure, $\times 1000$; (b) structure of AlCoCrCuFeNi layer—cBNCoMo layer, $\times 300$; (c) structure of AlCoCrCuFeNi layer—B4CCoMo layer, $\times 500$; (d) AlCoCrCuFeNi layer structure, $\times 30,000$; (e) cBNCoMo layer structure, $\times 100,000$; (f) B4CCoMo layer structure, $\times 150,000$.

Figure 3a,b show the structure of the Hastelloy X (NiCrFeMo)—AlCoCrCuFeNi—cBNCoMo composite. Figure 3a shows an enlarged part of the structure (the interface between the Hastelloy X (NiCrFeMo) and AlCoCrCuFeNi alloy layers) of the Hastelloy X (NiCrFeMo)—AlCoCrCuFeNi—cBNCoMo composite. Figure 3b shows an enlarged part of the structure (the interface between the AlCoCrCuFeNi and cBNCoMo alloy layers) of the Hastelloy X (NiCrFeMo)—AlCoCrCuFeNi—cBNCoMo composite. Figure 3c shows an enlarged part of the structure (the interface between the AlCoCrCuFeNi and B4CCoMo alloy layers) of the Hastelloy X (NiCrFeMo)—AlCoCrCuFeNi—B4CCoMo composite.

We studied the structure of AlCoCrCuFeNi, cBNCoMo, and B4CCoMo after complex processing, including high-energy mechanical processing of materials and HVOF in a protective atmosphere, followed by thermomechanical treatment (Figure 4a–c). The results of X-ray diffraction showed that the high-entropy AlCoCrCuFeNi layer consists of ordered and disordered body-centered cubic (BCC) phases, a small number of face-centered cubic (FCC) phases, and austenitic B2 cubic phases (Figure 4a). The cBNCoMo ceramic layer consists of BN cubic phase, Co hexagonal phase, B2CN orthorhombic phase, and Mo cubic phase (Figure 4b). The B4CCoMo ceramic layer consists of B4C phases with rhombohedral lattice, Co phases with hexagonal lattice, B4C2Co22 phases with cubic lattice, and Mo with cubic lattice (Figure 4c).

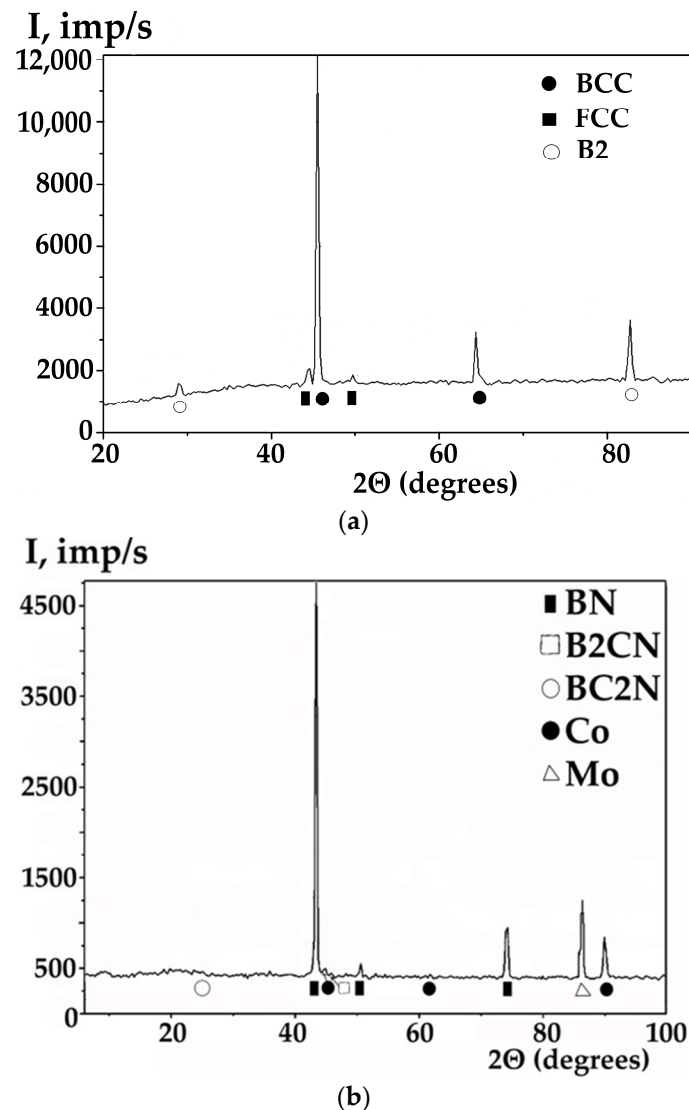


Figure 4. Cont.

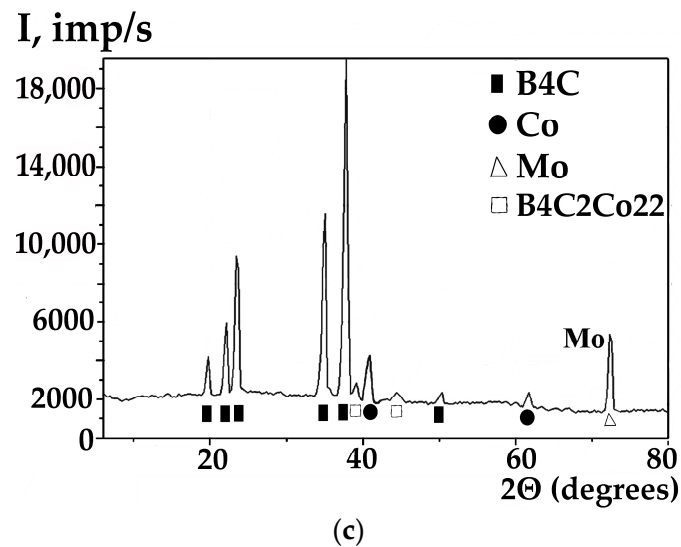


Figure 4. X-ray diffraction patterns of hybrid composite materials: (a) AlCoCrCuFeNi; (b) cBNCoMo; (c) B4CCoMo.

The structural parameters of the alloy crystal lattices of AlCoCrCuFeNi, cBNCoMo, and B4CCoMo alloys included in the hybrid composite materials are presented in Table 2.

Table 2. Structural parameters of the alloy crystal lattices included in the hybrid composite materials.

Phase	a, nm	$V_{at} \cdot 10^3$	b, nm	c, nm	β , Degrees
cBNCoMo					
BN (cubic)	0.3615	47.24	0.3615	0.3615	90.00
B2CN (hexagonal)	0.2574	25.49	0.2574	0.4442	90.00
B2CN (orthorhombic)	0.256	50.77	0.791	0.2507	90.00
Co (hexagonal)	0.2503	25.44	0.2503	0.406	90.00
B4CCoMo					
B4 C (rhombohedral)	0.5593	378.039	0.5593	1.2085	90.00
B4 C2 Co22 (cubic)	1.046	1144.445	1.046	1.046	90.00
Co (hexagonal)	0.2502	25.35	0.2502	0.405	90.00
AlCoCrCuFeNi					
BCC (body-centered cubic lattice)	0.2875	23.76	0.2875	0.2875	90.00
FCC (face-centered cubic lattice)	0.3608	46.97	0.3608	0.3608	90.00
B2 (cubic)	0.3207	32.98	0.3207	0.3207	90.00

The microhardnesses of Hastelloy X (NiCrFeMo)—AlCoCrCuFeNi—cBNCoMo and Hastelloy X (NiCrFeMo)—AlCoCrCuFeNi—B4CCoMo are: super alloy Hastelloy X (NiCrFeMo) $HV_{0.2} = 3.8 \div 3.95$ GPa; alloy AlCoCrCuFeNi $HV_{0.2} = 4.41 \div 4.57$ GPa; alloy cBNCoMo, $HV_{0.3} = 34.3 \div 34.8$ GPa; and alloy B4CCoMo, $HV_{0.3} = 18.7 \div 18.9$ GPa (Figure 5). The data on the distribution of layer-by-layer changes in microhardness, as well as information on their maximum values, suggest that such “layered structures” increase the mechanical characteristics of the material and, in particular, make them strong and wear-resistant.

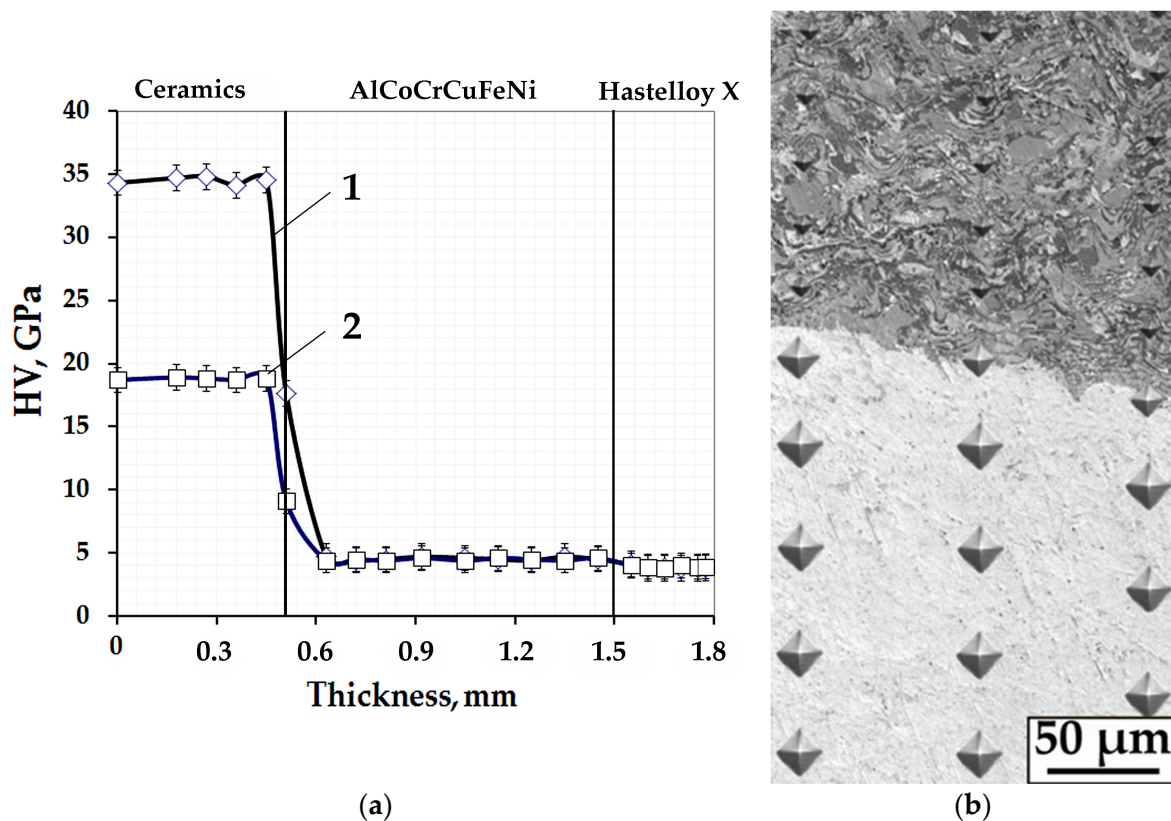


Figure 5. (a) Microhardness of composite materials: Hastelloy X (NiCrFeMo)—AlCoCrCuFeNi—cBNCoMo (1); Hastelloy X (NiCrFeMo)—AlCoCrCuFeNi—B₄CCoMo (2); (b) Photograph of measuring the microhardness of composite material AlCoCrCuFeNi—cBNCoMo.

We chose cubic boron nitride and boron carbide as hard materials for functional hybrid composite layers. Cubic boron nitride and boron carbide, unlike other superhard materials, are not subjected to chemical wear, i.e., they are chemically neutral. We took cobalt and molybdenum as binding materials. The data analysis allowed us to conclude that binders based on Co and Mo at a content of 10–30% have the best set of mechanical properties and adhesion, while cohesion is up to cBN grains. Taking into account the chemical affinity of Co with the AlCoCrCuFeNi functional layer and its scarcity, we used 10% Co as a binder.

3.3. Performance Properties of Surface-Modified Composite Materials

Experience shows that the optimization of composite materials increases the following characteristics: strength, hardness, durability, and wear resistance. During the wear test of samples layered with AlCoCrCuFeNi—cBNCoMo and AlCoCrCuFeNi—B₄CCoMo, the temperature in the friction zone increased. The increase in wear resistance can be explained by the increased hardness of the cBNCoMo and B₄CCoMo layers.

The endurance limit of Hastelloy X (NiCrFeMo) alloy was 340 MPa, the endurance limit of the AlCoCrCuFeNi—cBNCoMo layers was 410 MPa, and the endurance limit of the AlCoCrCuFeNi—B₄CCoMo layers was 385 MPa (Figure 6a).

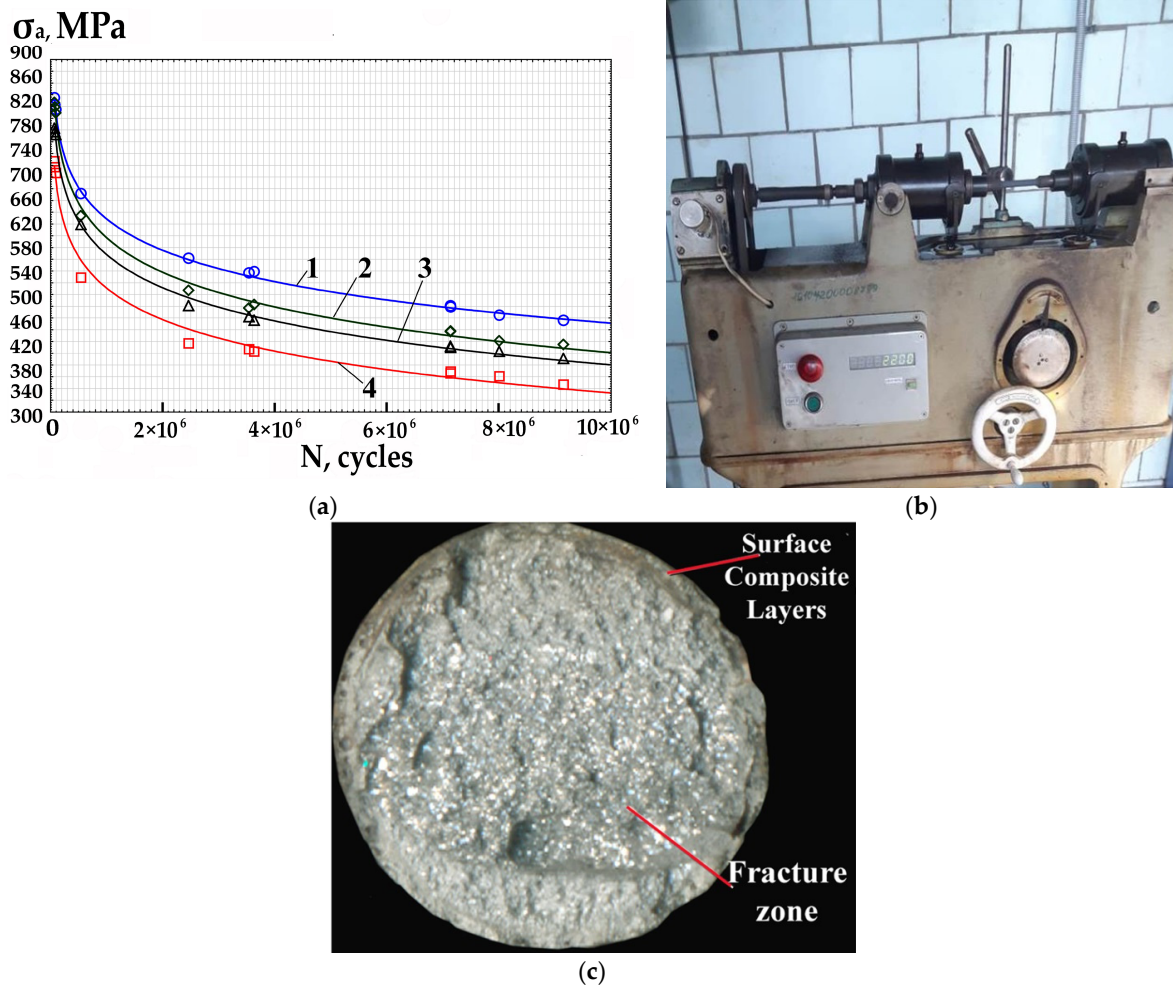


Figure 6. (a) Multi-cycle fatigue curves of Hastelloy X (NiCrFeMo): without coating (4), after surface modification with composite material AlCoCrCuFeNi—B4CCoMo ($\delta \approx 1.5$ mm) (3); after surface modification with composite material AlCoCrCuFeNi—cBNCoMo ($\delta \approx 1.5$ mm) (2); after surface modification with composite material NiCoTiZrHf—cBNCoMo ($\delta \approx 1.5$ mm) (1); (b) photographs of multi-cycle fatigue tests; (c) photograph of destruction of a sample from a composite material as a result of mechanical tests for high-cycle fatigue.

As a result of the statistical processing of experimental data, empirical Equations (3)–(6) of stress amplitude dependence (σ_a) on cyclic durability value (N) were obtained in the program Statistics 10.0:

$$\text{Hastelloy X (NiCrFeMo): } \sigma_a = 681.97 - 9.94 \times 10^{-5} \times N + 6.96 \times 10^{-12} \times N^2, \quad (3)$$

$$\text{AlCoCrCuFeNi—B4CCoMo: } \sigma_a = 750.31 - 0.0001 \times N + 7.11 \times 10^{-12} \times N^2 \quad (4)$$

$$\text{AlCoCrCuFeNi—cBNCoMo: } \sigma_a = 785.95 - 0.0001 \times N + 7.52 \times 10^{-12} \times N^2, \quad (5)$$

$$\text{NiCoTiZrHf0151—cBNCoMo: } \sigma_a = 798.3 - 9.14 \times 10^{-5} \times N + 5.93 \times 10^{-12} \times N^2, \quad (6)$$

Figure 7a shows the results of friction-wear tests of composite materials: NiCoTiZrHf + cBNCoMo; AlCoCrCuFeNi—cBNCoMo; AlCoCrCuFeNi—B4CCoMo; and Hastelloy X (NiCrFeMo). The total thickness of the composite layers was 1.5 mm. The samples obtained were tested on a friction-wear testing machine 2070 CMT-1 (Figure 7b) according to the disk–disk scheme. The tests were carried out under dry friction conditions at a disk sliding speed of 2 m/s. During loading, the temperature at the contact point

was measured. The experimental data were processed using the Statistica v10.0 application package in the SPSS environment. The analysis of the results obtained shows (Figure 7a) that material Hastelloy X (NiCrFeMo) ($I = 46.16 \times 10^{-6}$ g/m, disk pressure $P = 9.4$ MPa) has the highest wear rate (Figure 7a, curve 1). Meanwhile, the lowest wear rate belongs to the composite material AlCoCrCuFeNi—B4CCoMo ($I = 30.82 \times 10^{-6}$ g/m, disk pressure $P = 9.4$ MPa) (Figure 7a, curve 2). The wear rates of the composite materials are as follows: AlCoCrCuFeNi—cBNCoMo ($I = 27.78 \times 10^{-6}$ g/m, disk pressure $P = 9.4$ MPa) (Figure 7a, curve 3) and NiCoTiZrHf3—cBNCoMo ($I = 24.43 \times 10^{-6}$ g/m, disk pressure $P = 9.4$ MPa) (Figure 7a, curve 4).

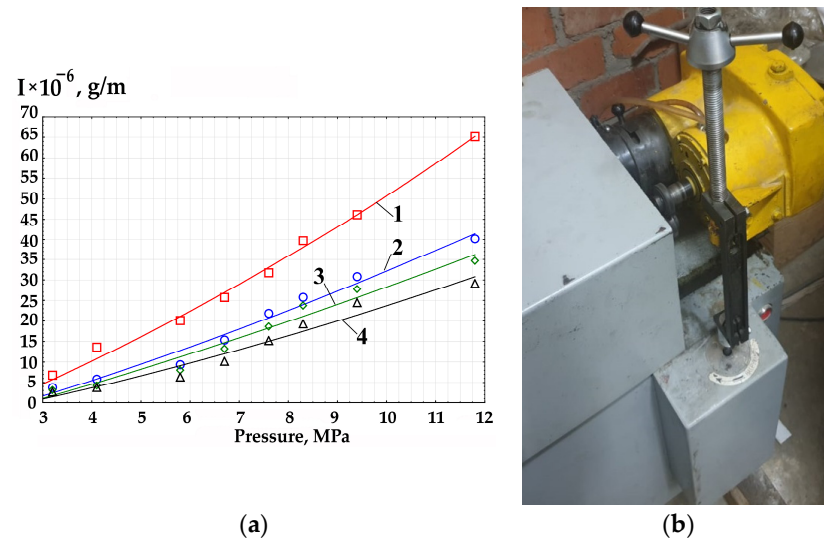


Figure 7. (a) Dependence of the wear intensity I on the pressure of the disk P : the sliding speed of the disk: NiCoTiZrHf—cBNCoMo—4; AlCoCrCuFeNi—cBNCoMo—3; AlCoCrCuFeNi—B4CCoMo—2; Hastelloy X (NiCrFeMo)—1; sliding speed of the disk—2 m/s; (b) photograph of the friction-wear test.

The wear rate (I) from the pressure (P) of the disk changes according to polynomial dependence (Figure 6a) and is described by empirical Equations (7)–(10). The equations were obtained from the mathematical analysis of experimental data using Statistica v10.0 software:

$$\text{AlCoCrCuFeNi—B4CCoMo: } I = -8.77 + 3.202 \times P + 0.089 \times P^2, \quad (7)$$

$$\text{Hastelloy X (NiCrFeMo): } I = -10.07 + 4.4 \times P + 0.168 \times P^2, \quad (8)$$

$$\text{AlCoCrCuFeNi—cBNCoMo: } I = -8.86 + 3.12 \times P + 0.06 \times P^2, \quad (9)$$

$$\text{NiCoTiZrHf—cBNCoMo: } I = -6.57 + 2.25 \times P + 0.08 \times P^2 \quad (10)$$

The positive results of the wear and fatigue tests give grounds to recommend Hastelloy X (NiCrFeMo)—AlCoCrCuFeNi—cBNCoMo and Hastelloy X (NiCrFeMo)—AlCoCrCuFeNi—B4CCoMo to improve various structural elements working in the oil and gas industry. These layers are able to provide special properties of high entropy. They are also able to improve ceramic materials and increase their damping capacity and crack resistance. The increased crack resistance of Hastelloy X (NiCrFeMo)—AlCoCrCuFeNi—cBNCoMo and Hastelloy X (NiCrFeMo)—AlCoCrCuFeNi—B4CCoMo is explained by the increased properties of high-entropy materials. This has been confirmed by a number of studies. The nanostructural state makes the composite adaptable to operating conditions. Thus, the considered composites Hastelloy X (NiCrFeMo)—AlCoCrCuFeNi—cBNCoMo and Hastelloy X (NiCrFeMo)—AlCoCrCuFeNi—B4CCoMo can be classified as smart, self-adaptive, and widely demanded in various branches of technology, including potentially dangerous conditions. These materials actively counteract external influences, reduce vibrations, and redistribute mechanical stresses.

4. Discussion

4.1. High-Temperature Thermomechanical Treatment of Layered Composite Materials

In order to increase the adhesion and cohesion of the AlCoCrCuFeNi, cBNCoMo, and B4CCoMo layers of Hastelloy X (NiCrFeMo)—AlCoCrCuFeNi—cBNCoMo and Hastelloy X (NiCrFeMo)—AlCoCrCuFeNi—B4CCoMo, we carried out high-temperature treatment. High-temperature treatment of AlCoCrCuFeNi, cBNCoMo, and B4CCoMo increases adhesive and cohesive strength up to 162–183 MPa. During high-temperature thermomechanical processing, we can observe high compressive forces between the layers. These forces lead to welding of the composite layers.

After HVOF treatment of the composite layers, we carried out high-temperature treatment. It included surface plastic deformation at temperatures of 1223–1323 K, followed by annealing at temperatures of 973–1073 K for 1 h. HVOF treatment of AlCoCrCuFeNi, cBNCoMo, and B4CCoMo leads to a high density of crystal lattice defects and internal stresses (first stresses or residual stresses). Their magnitude and nature are determined by the deposited materials and the deposition conditions. Internal stresses prevent the mobility of twinning boundaries. They can decrease the functional and mechanical properties of the resulting layers and cause cracking or peeling of the layers from the base (Hastelloy X (NiCrFeMo)) [2,44,45]. To improve the characteristics of the layered composite materials, we carried out annealing. This procedure causes relaxation of internal stresses in the layers of hybrid composites [2,46,47]. Adhesive strength also increases during thermomechanical treatment due to the intensified diffusion processes at the boundary “Hastelloy X (NiCrFeMo)—AlCoCrCuFeNi alloy layer”. The main purpose of heat treatment was to stabilize the structure (eliminate unwanted intermetallic phases) and increase functional properties with the maximum possible relaxation of residual internal stresses after the deposition of AlCoCrCuFeNi, cBNCoMo, and B4CCoMo alloys. During heat treatment (annealing), the structure of the layers, like that of a superalloy, undergoes changes: the grain size increases in a small range, and its overall effect also affects the microhardness of materials, which are “sensitive” to structural changes. There is also some “softening” of the alloys. Thus, we can conclude that annealing affects the structure, microhardness, composition, and elimination of the chemical inhomogeneity of AlCoCrCuFeNi, cBNCoMo, and B4CCoMo. This, in turn, has a favorable effect on the functional properties of hybrid composites.

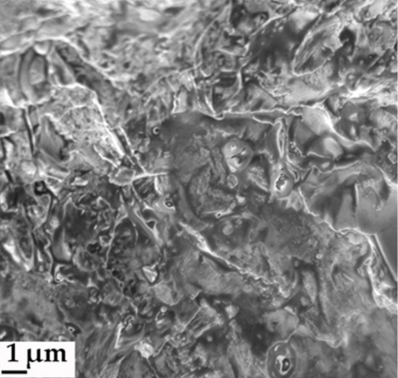
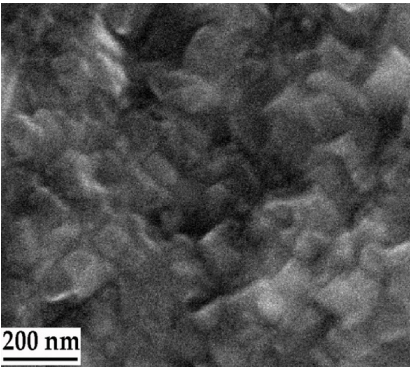
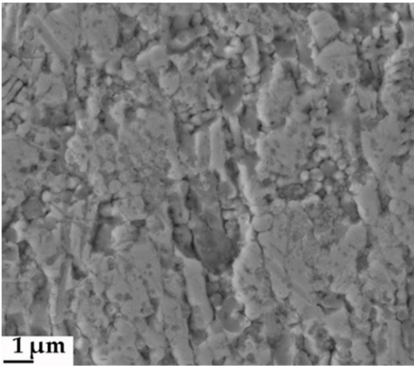
The operating conditions in tribosystems, i.e., conditions of friction and wear, occur when the surface layers of the contacting parts experience energy effects and are in a complex stress–strain state. Static and dynamic loads cause high internal stresses and elastic and plastic deformations. All these factors lead to fatigue and wear of the surface layer [48–50]. The main requirement for materials operating in such conditions is multifunctionality. During operation, materials must withstand high specific loads, sliding speeds, and thermal and force deformations. They must also have sufficient mechanical strength, friction coefficient stability, run-in resistance, seizing resistance, high wear resistance, corrosion resistance, and low cost [15,16,21,22].

4.2. Multifunctional Surface Compositions “AlCoCrCuFeNi—cBNCoMo” and “AlCoCrCuFeNi—B4CCoMo”

The priority direction in materials for the oil and gas industry is the use of smart, intermetallic, nanocrystalline, and layered materials with improved properties. The use of high-entropy materials as surface layers or as part of a layered structure can provide an effective response of materials to external factors. Directional intellectualization of composite materials increases the stability of tribological properties. The use of micro- and nanotechnologies provides self-diagnosis and adaptation to external influences. In recent years, a large amount of research has been carried out to develop innovative types of layered composites. These composites, in terms of structure, architecture, and properties, improve the products for various purposes. In order to ensure the multifunctionality of a surface composition operating under conditions of cyclic loading and reverse friction, it is

important to correctly design its outer layers. These layers perceive external influences as, for example, does a layer of increased wear resistance [2,15,16,21,22]. In Table 3, we have shown one of the options for a composite surface layer for operation in cyclic loading and reverse friction. We have also demonstrated the requirements and technological efficiency of the constituent layers of the composition.

Table 3. Multilayer hybrid composite material operating under cyclic loading and reverse friction requirements and technological efficiency of functional layers.

Functional Layers	Requirements	Efficiency
 <p data-bbox="118 999 496 1055">Layer of high-energy wear-resistant material cBNCoMo</p>	<ul style="list-style-type: none"> - high wear resistance; - minimization of physical and chemical interaction with the environment; - optimal hardness and passivation of tribological interaction. 	<ul style="list-style-type: none"> - high strength; - optimal hardness; - high wear resistance; - increased corrosion resistance; - passivation of tribological interaction.
 <p data-bbox="118 1467 443 1523">Layer of high-entropy material AlCoCrCuFeNi</p>	<ul style="list-style-type: none"> - chemical and phase composition ensures the martensitic state of the layer of SME material under operating conditions; crystal chemical interaction of adjacent layers. 	<ul style="list-style-type: none"> - increase in cyclic durability due to braking or blocking crack propagation; relaxation of thermomechanical stresses at the layer boundary.
 <p data-bbox="118 1935 549 1968">Base (Superalloy Hastelloy X(NiCrFeMo))</p>	<ul style="list-style-type: none"> - increased strength; - high crack resistance; - heat treatment providing an optimal level of residual stresses. 	<ul style="list-style-type: none"> - increased fatigue strength, cyclic durability, and crack resistance.

In order to ensure functional and mechanical properties, the architecture of multilayer hybrid composite materials is designed as follows: the underlying AlCoCrCuFeNi layer

must provide high load-bearing capacity and damping under mechanical or thermal impact. To increase the durability and survivability of the product under friction–fatigue cyclic loading, it is advisable to use a functional layer of ceramic materials, such as cBNCoMo or B4CCoMo, which have stable high corrosion–fatigue strength under operating conditions.

The multilayer compositions Hastelloy X (NiCrFeMo)—AlCoCrCuFeNi—cBNCoMo and Hastelloy X (NiCrFeMo)—AlCoCrCuFeNi—B4CCoMo are characterized by higher energy absorption than single-layer coatings, a decrease in the propagation rate of microcracks in layers with a gradient in phase composition and thicknesses, high adhesive properties of the constituent layers and the base, and wider technological capabilities in the selection of the connecting layer [2,15,16,21,22].

The formation of hybrid composite materials at all stages was carried out under conditions of complex, high-energy effects. This allowed us to obtain materials with an increased combination of functional and mechanical properties. However, for successful processing, it is necessary to “synchronize” the parameters of all the influence methods on the material, taking into account technological inheritance, and to optimize the processing parameters to obtain qualitatively new structures and structure-sensitive properties. This process is an important research step in the development of the structure and architecture of composites.

Nanostructured particles experience high contact pressure during plastic deformation of layered composite materials under high-temperature treatment. As a result, particles decrease in the ratio 1:8.6. The energy stored in the process of high-energy machining in the form of various kinds of defects releases. This leads to a better connection of the sprayed particles with each other and with the base, i.e., provides good adhesive properties and lower porosity. Meanwhile, the high-temperature gradient between the substrate and the powder particles creates additional conditions for nanostructuring. Crystallization during high-temperature thermomechanical treatment forms nuclei on long-range order fluctuations. Their number and size can be determined by the degree of cooling. When the layers of composite materials are cooled, crystallization proceeds under conditions of heat deficiency, and the temperature at the front of the growing crystal drops sharply. As a result, crystals cease to grow at a certain stage. Meanwhile, the melt, which remains untransformed, solidifies and forms an amorphous state. The amorphous component, after hot plastic deformation, subsequently undergoes dynamic recrystallization and forms nanoscale structures [2,51–53].

Samples with AlCoCrCuFeNi—cBNCoMo and AlCoCrCuFeNi—B4CCoMo layers become more durable because nanostructured materials are destructed. Destruction stops at grain boundaries and prevents branching and movement of cracks, and boundaries harden.

5. Conclusions

Hybrid composite materials can successfully solve the problems of reliability, durability, and extended functionality of products, components, and details, which operate under conditions of multifactorial influences (temperature, force, and deformation). The authors developed the technology of hybrid composites, including layers of high-entropy materials and layers of ceramic materials. The developed technology includes high-energy machining, high-velocity oxygen-fuel spraying in a protective environment, high-temperature thermomechanical treatment, and heat treatment.

As a result of the research, the following tasks were solved:

1. We increased the adhesive strength of the composite layers from 68 to 192 MPa with the developed technology.
2. We substantiated the choice of powder materials for the formation of high-entropy AlCoCrCuFeNi and ceramic cBNCoMo(B4CCoMo) layers of composites to increase the reliability and durability of the products.
3. We improved the adhesive properties and quality (reduction of porosity) of composite layers using high-energy processing of AlCoCrCuFeNi, cBNCoMo, and B4CCoMo powder materials.

4. We developed statistical models for optimizing the technological parameters for the formation of composite materials.
5. We described the technological regimens of high-temperature thermomechanical treatment in order to improve the mechanical properties of composites (adhesion).
6. We studied the structure of AlCoCrCuFeNi, cBNCoMo, and B4CCoMo composites after complex processing. The studies show that the AlCoCrCuFeNi layer has a grain size of 75–123 nm, the cBNCoMo layer has a grain size of 92–136 nm, and the B4CCoMo layer has a grain size of 86–163 nm. The microhardness was Hastelloy X (NiCrFeMo) HV = $3.8 \div 3.95$ GPa; AlCoCrCuFeNi HV = $4.41 \div 4.57$ GPa; cBNCoMo, HV = $34.3 \div 34.8$ GPa; and B4CCoMo, HV = $18.7 \div 18.9$ GPa.
7. We performed mechanical tests of hybrid composites Hastelloy X (NiCrFeMo)—AlCoCrCuFeNi—cBNCoMo and Hastelloy X (NiCrFeMo)—AlCoCrCuFeNi—B4CCoMo for cyclic durability (fatigue mechanical tests) and friction wear. The tests show that the endurance limit of Hastelloy X (NiCrFeMo) alloy samples was 340 MPa, with AlCoCrCuFeNi—cBNCoMo composite surface layers of 410 Mpa and AlCoCrCuFeNi—B4CCoMo composite surface layers of 385 MPa. The use of surface-layered materials AlCoCrCuFeNi—cBNCoMo and AlCoCrCuFeNi—B4CCoMo in the composition of hybrid composites increases cyclic durability.

The use of surface-layered materials in the composition of hybrid composites made it possible to significantly reduce the wear rate from $I = 46.16 \times 10^{-6}$ g/m (for Hastelloy X (NiCrFeMo)) to $I = 27.78 \times 10^{-6}$ g/m (AlCoCrCuFeNi—cBNCoMo).

The test results show that the developed composites are promising for use in various industries (including oil and gas), where high strength and wear resistance of materials are required.

Author Contributions: Conceptualization, P.R. and Z.B.; methodology, P.R., Z.B., A.R. and G.K.; software, P.R., A.R., G.K. and M.S.; validation, P.R., Z.B., A.R., G.K. and M.S.; formal analysis, P.R., A.R. and G.K.; investigation, P.R. and Z.B.; resources, P.R., A.R., G.K. and M.S.; data curation, P.R., A.R. and G.K.; writing—original draft preparation, P.R.; writing—review and editing, P.R. and Z.B.; visualization, G.K. and M.S.; supervision, P.R., A.R. and G.K.; project administration, P.R.; funding acquisition, P.R. All authors have read and agreed to the published version of the manuscript.

Funding: This research was funded by Russian Scientific Foundation grant number 23-23-00074.

Data Availability Statement: The data presented in this study are available on request from the corresponding author.

Acknowledgments: The work was done under the financial support of the Russian Scientific Foundation No. 23-23-00074.

Conflicts of Interest: The authors declare no conflict of interest.

References

1. Sagalovych, A.; Sagalovych, V.; Popov, V.; Dudnik, S. *Vacuum-Plasma Multilayer Protective Coatings for Turbine Blades*; Scientific Route OÜ: Tallinn, Estonia, 2021; 104p. [\[CrossRef\]](#)
2. Blednova, Z.M.; Rusinov, P.O. *Promising Materials and Technologies: Formation of Multifunctional Surface Compositions from High-Entropy Alloys with Thermoelastic Martensitic Transformations*; Rubanik, V.V., Ed.; BSU Publishing Center: Minsk, Belarus, 2021; 658p.
3. Duchaniya, R.K.; Pandel, U.; Rao, P. Coatings based on high entropy alloys: An overview. *Mater. Today Proc.* **2021**, *44*, 4467–4473. [\[CrossRef\]](#)
4. Lin, C.; Yao, Y. Corrosion-Resistant Coating Based on High-Entropy Alloys. *Metals* **2023**, *13*, 205. [\[CrossRef\]](#)
5. Fu, M.; Ma, X.; Zhao, K.; Li, X.; Su, D. High-entropy materials for energy-related applications. *iScience* **2021**, *24*, 102177. [\[CrossRef\]](#) [\[PubMed\]](#)
6. Ma, Y.; Ma, Y.; Wang, Q.; Schweidler, S.; Botros, M.; Fu, T.; Hahn, H.; Brezesinski, T.; Breitung, B. High-entropy energy materials: Challenges and new opportunities. *Energy Environ. Sci.* **2021**, *14*, 2883. [\[CrossRef\]](#)
7. Mehmood, M.A.; Shehzad, K.; Mujahid, M.; Yaqub, T.B.; Godfrey, A.; Fernandes, F.; Muhammad, F.Z.; Yaqoob, K. Ceramic-reinforced HEA matrix composites exhibiting an excellent combination of mechanical properties. *Sci. Rep.* **2022**, *12*, 21486. [\[CrossRef\]](#) [\[PubMed\]](#)

8. Medina, L.Z.; Riekehr, L.; Jansson, U. Phase formation in magnetron sputtered CrMnFeCoNi high entropy alloy. *Surf. Coat. Technol.* **2020**, *403*, 126323. [[CrossRef](#)]
9. Moghaddam, A.O.; Shaburova, N.A.; Samodurova, M.N.; Abdollahzadeh, A.; Trofimov, E.A. Additive manufacturing of high entropy alloys: A practical review. *J. Mater. Sci. Technol.* **2021**, *77*, 131–162. [[CrossRef](#)]
10. Ananiadis, E.; Argyris, K.T.; Matikas, T.E.; Sfikas, A.K.; Karantzalis, A.E. Microstructure and Corrosion Performance of Aluminium Matrix Composites Reinforced with Refractory High-Entropy Alloy Particulates. *Appl. Sci.* **2021**, *11*, 1300. [[CrossRef](#)]
11. Akrami, S.; Edalati, P.; Fuji, M.; Edalati, K. High-entropy ceramics: Review of principles, production and applications. *Mater. Sci. Eng. R Rep.* **2021**, *146*, 100644. [[CrossRef](#)]
12. Chang, Y.; Sun, X.; Ma, M.; Mu, C.; Li, P.; Li, L.; Li, M.; Nie, A.; Xiang, J.; Zhao, Z.; et al. Application of hard ceramic materials B₄C in energy storage: Design B₄C@C core-shell nanoparticles as electrodes for flexible all-solid-state micro-supercapacitors with ultrahigh cyclability. *Nano Energy* **2020**, *75*, 104947. [[CrossRef](#)]
13. Kara, M.; Coskun, T.; Gunoz, A. Influence of B₄C on enhancing mechanical properties of AA2014 aluminum matrix composites. *Part C J. Mech. Eng. Sci.* **2021**, *236*, 5. [[CrossRef](#)]
14. Makhutov, N.A.; Matvienko, Y.G.; Blednova, Z.M.; Rusinov, P.O.; Dmitrenko, D.V. The effect of surface coating by shape memory alloys on mechanical properties of steel. *Fatigue Fract. Eng. Mater. Struct.* **2022**, *45*, 1550–1553. [[CrossRef](#)]
15. Rusinov, P.O.; Blednova, Z.M.; Kurapov, G.V. Functionally-oriented composite layered materials with martensitic transformations. *Surf. Innov.* **2023**, *11*, 26–37. [[CrossRef](#)]
16. Rusinov, P.O.; Blednova, Z.M. Physicomechanical and design characteristics of surface high-entropy alloys. *Part L J. Mater. Des. Appl.* **2021**, *235*, 1635–1644. [[CrossRef](#)]
17. Yang, L.; Shi, X.; Tian, X.; Wang, H.; Qi, L. Microstructure and corrosion behavior of ZrO₂ coated carbon fiber reinforced magnesium matrix composites sprayed with different powder characteristics. *Ceram. Int.* **2022**, *48*, 30797–30806. [[CrossRef](#)]
18. Mostafa, H.; Sliem, O.F.; Shakoor, R.A.; Bagheridard, S.; Mansoor, B.; Abdullah, A.; Mohamed, A.; Mohamed, A. The influence of different preparation methods on the erosion behavior of NiP-ZrO₂ nanocomposite coating. *Tribol. Int.* **2023**, *178*, 108014. [[CrossRef](#)]
19. Kim, S.; Kim, T.; Hong, E.; Jo, I.; Kim, J.; Lee, H. Phase Formation and Wear Resistance of Carbon-Doped TiZrN Nanocomposite Coatings by Laser Carburization. *Metals* **2021**, *11*, 590. [[CrossRef](#)]
20. Lee, D.; Kim, J.; Park, B.; Jo, I.; Lee, S.K.; Kim, Y.; Lee, S.B.; Cho, S. Mechanical and Thermal Neutron Absorbing Properties of B₄C/Aluminum Alloy Composites Fabricated by Stir Casting and Hot Rolling Process. *Metals* **2021**, *11*, 413. [[CrossRef](#)]
21. Blednova, Z.M.; Makhutov, N.A.; Rusinov, P.O.; Dmitrienko, D.V.; Balaev, E.Y. Analysis of the Efficiency of Functionally Oriented Composite Coatings Made of Materials with Thermoelastic Martensitic Transformations. *Russ. Metall.* **2021**, *2021*, 1224–1232. [[CrossRef](#)]
22. Rusinov, P.O.; Blednova, Z.M. Study of the structure and properties of a high-entropy ceramic composite material. *Surf. Innov.* **2022**, *10*, 217–226. [[CrossRef](#)]
23. Cai, X.; Zhang, N.; Liu, H. Thickness dependence of viscoelastic stress relaxation of laminated microbeams due to mismatch strain. *Appl. Math. Mech.* **2022**, *43*, 467–478. [[CrossRef](#)]
24. Maleki, E.; Unal, O.; Guagliano, M.; Bagherifard, S. Analysing the Fatigue Behaviour and Residual Stress Relaxation of Gradient Nano-Structured 316L Steel Subjected to the Shot Peening via Deep Learning Approach. *Met. Mater. Int.* **2022**, *28*, 112. [[CrossRef](#)]
25. Duan, Y.J.; Qiao, J.C.; Wada, T.; Kato, H.; Pineda, E.; Crespo, D.; Wang, Y.J. Stress relaxation in high-entropy Pd₂₀Pt₂₀Cu₂₀Ni₂₀P₂₀ metallic glass: Experiments, modeling and theory. *Mech. Mater.* **2021**, *160*, 103959. [[CrossRef](#)]
26. Lee, S.; Duarte, M.J.; Feuerbacher, M.; Soler, R.; Kirchlechner, C.; Liebscher, C.H.; Oh, S.H.; Dehm, G. Dislocation plasticity in FeCoCrMnNi high-entropy alloy: Quantitative insights from in situ transmission electron microscopy deformation. *Mater. Res. Lett.* **2020**, *8*, 6. [[CrossRef](#)]
27. Rozman, K.A.; Detrois, M.; Liu, T.; Gao, M.C.; Jablonski, P.D.; Hawk, J.A. Long-Term Creep Behavior of a CoCrFeNiMn High-Entropy Alloy. *J. Mater. Eng. Perform.* **2020**, *29*, 5822–5839. [[CrossRef](#)]
28. Campari, E.G.; Casagrande, A. Mechanical Spectroscopy Study of CrNiCoFeMn High-Entropy Alloys. *Materials* **2023**, *16*, 3689. [[CrossRef](#)]
29. Belov, M.M.; Ivanov, I.A.; Uglov, V.V.; Zlotski, S.V.; Jin, K.; Stepanjuk, N.A.; Ryskulov, A.E.; Kozlovskiy, A.L.; Koloberdin, M.V.; Kurakhmedov, A.E.; et al. Stress evolution in NiCoFeCrMn and NiCoFeCr high-entropy alloys irradiated by helium and krypton ions. In Proceedings of the 8th International Congress on Energy Fluxes and Radiation Effects (EFRE-2022), Tomsk, Russia, 29–30 September 2022; pp. 1082–1087. [[CrossRef](#)]
30. Duan, Y.J.; Zhang, L.T.; Qiao, J.C.; Wang, Y.J.; Yang, Y.; Wada, T.; Kato, H.; Pelletier, J.M.; Pineda, E.; Crespo, D. Intrinsic Correlation between the Fraction of Liquidlike Zones and the β Relaxation in High-Entropy Metallic Glasses. *Phys. Rev. Lett.* **2022**, *129*, 175501. [[CrossRef](#)]
31. Liu, W.; Otegi, N.; Orallo, A.; Barrenetxea, M.; Aizpuru, I.; Lian, J.; Mendiguren, J. Post-forming, electro-plastic effect internal stress reduction in AA5754 aluminium alloy. *Mater. Sci. Eng. A* **2022**, *852*, 143686. [[CrossRef](#)]
32. Lee, Y.S.; Sung, J.H. Microstructure and Mechanical Properties of Hastelloy X Fabricated Using Directed Energy Deposition. *Metals* **2023**, *13*, 885. [[CrossRef](#)]
33. Liu, M.; Zeng, Q.; Hua, Y.; Zheng, W.; Wu, Y.; Jin, Y.; Li, Y.; Wang, J.; Zhang, K. High-Temperature Tensile Properties of Hastelloy X Produced by Laser Powder Bed Fusion with Different Heat Treatments. *Metals* **2022**, *12*, 1435. [[CrossRef](#)]

34. Wang, H.; Wu, H.; Liu, Y.; Qiu, W.; Deng, H.; Zhou, L.; Chen, L. Oxidation Behavior of Hastelloy X Alloy Fabricated by Selective Laser Melting and Subsequent Hot Isostatic Pressing Treatment. *Adv. Eng. Mater.* **2022**, *24*, 2200369. [[CrossRef](#)]
35. Baranowski, M.; Senkara, J. Mechanical Properties of Structural Components in Hastelloy X Joints Brazed with Ni-Pd-Cr-B-Si Alloy. *Materials*. **2023**, *16*, 1115. [[CrossRef](#)]
36. Yin, W.; Ruidi, L.; Pengda, N.; Zhijian, Z.; Tiechui, Y.; Jiwei, Y.; Kun, L. Microstructures and properties of equimolar AlCoCrCuFeNi high-entropy alloy additively manufactured by selective laser melting. *Intermetallics* **2020**, *120*, 106746. [[CrossRef](#)]
37. Prabu, G.; Duraiselvam, M.; Jeyaprakash, N.; Yang, C.-H. Microstructural Evolution and Wear Behavior of AlCoCrCuFeNi High Entropy Alloy on Ti-6Al-4V Through Laser Surface Alloying. *Met. Mater. Int.* **2021**, *27*, 2328–2340. [[CrossRef](#)]
38. Bian, C.H.; Yang, W.J.; Zhang, W.; Li, Q.; Wen, J.; Feng, L. Analysis of the effect of FeCr phase and AlCo phase in the friction process of AlCoCrCuFeNi high entropy alloy coating. *J. Lanzhou Univ. Technol.* **2023**, *49*, 9–16.
39. Kuznetsov, A.V.; Shaisultanov, D.G.; Stepanov, N.; Salishchev, G.A.; Senkov, O.N. Superplasticity of AlCoCrCuFeNi High Entropy Alloy. *Mater. Sci. Forum* **2012**, *735*, 146–151. [[CrossRef](#)]
40. Plevachuk, Y.; Brillo, J.; Yakymovych, A. AlCoCrCuFeNi-Based High-Entropy Alloys: Correlation Between Molar Density and Enthalpy of Mixing in the Liquid State. *Metall. Mater. Trans. A* **2018**, *49*, 6544. [[CrossRef](#)]
41. Veerasha, G.; Manjunatha, B.; Nagaral, M.; Auradi, V.; Bharath, V. Synthesis and wear behavior of varying particle sized B₄C reinforced Al2618 alloy composites. *Mater. Phys. Mech.* **2022**, *50*, 373. [[CrossRef](#)]
42. Velayatipour, O.; Nikzad, L.; Farvizi, M. B₄C reinforced NiTi-based composites: Microstructure and wear performance. *Appl. Ceram. Technol.* **2023**, *20*, 1667–1680. [[CrossRef](#)]
43. Bharathi, B.; Sampath, K.S. Mechanical Characteristics and Wear Behaviour of Al/SiC and Al/SiC/B₄C Hybrid Metal Matrix Composites Fabricated Through Powder Metallurgy Route. *Silicon* **2023**. online ahead of print. [[CrossRef](#)]
44. Li, Q. Quantification of Internal Stress and Cracking in Ambient Temperature Curing Thermoset Coatings. Ph.D. Thesis, Technical University of Denmark, Lyngby, Denmark, 2022; 136p.
45. Zhu, Y.; Zheng, B.; Hu, C.; Pei, H.; Song, P. Influence of Gradient Index and Pores on the Properties and Internal Stress of Continuous Transition Ceramic–Metal Coating. *Coatings* **2022**, *12*, 569. [[CrossRef](#)]
46. Rae, W.; Rahimi, S. Effect of stress relaxation on the evolution of residual stress during heat treatment of Ti-6Al-4V. *MATEC Web Conf.* **2020**, *321*, 11001. [[CrossRef](#)]
47. Lai, J.; Tran, D.; Yang, S.; Tseng, I.; Shie, K.; Leu, J.; Chen, C. Stress Relaxation and Grain Growth Behaviors of (111)-Preferred Nanotwinned Copper during Annealing. *Nanomaterials* **2023**, *13*, 709. [[CrossRef](#)]
48. Batra, N.K.; Dikshit, I.; Singh, R.P. Experimental Investigations and Statistical Modeling of Specific Wear and Coefficient of Friction in a Novel Carbon Fiber-Reinforced Composite. *Int. J. Surf. Eng. Interdiscip. Mater. Sci.* **2022**, *10*, 1–17. [[CrossRef](#)]
49. Juliá, J.M.; Rodríguez-Tembleque, L.; Ferri Aliabadi, M.H. Wear. In *Advanced Engineering Applications and Materials: Wear Modelling in Fibre-Reinforced Composite Materials*; World Scientific Publishing Europe Ltd.: Singapore, 2022; Chapter 8; pp. 205–236. [[CrossRef](#)]
50. Basu, B.; Kalin, M.; Manoj Kumar, B.V. *Friction and Wear of Ceramics: Principles and Case Studies*; John Wiley & Sons: Hoboken, NJ, USA, 2020; 400p.
51. Rodríguez-Ibabe, J.M.; Uranga, P. Thermomechanical Processing of Steels. *Metals* **2020**, *10*, 641. [[CrossRef](#)]
52. Feng, H.; Sun, Y.; Lian, Y.; Zhang, S.; Zhang, C.; Xu, Y.; Cao, P. Thermomechanical Processing of a Near- α Ti Matrix Composite Reinforced by TiBw. *Materials* **2020**, *13*, 5751. [[CrossRef](#)]
53. Rudskoi, A.I.; Kodzhaspirov, G.E.; Kliber, J.; Apostolopoulos, C.; Kitaeva, D.A. Physical Fundamentals of Thermomechanical processing in ultrafine-grained metallic materials manufacturing. *Mater. Phys. Mech.* **2020**, *43*, 50–58. [[CrossRef](#)]

Disclaimer/Publisher’s Note: The statements, opinions and data contained in all publications are solely those of the individual author(s) and contributor(s) and not of MDPI and/or the editor(s). MDPI and/or the editor(s) disclaim responsibility for any injury to people or property resulting from any ideas, methods, instructions or products referred to in the content.